Tropical Journal of Natural Product Research

Original Research Article

Synthesis, Characterization, and Anticancer Evaluation of Thiourea Benzamide Derivatives and their Cu(II) and Pt(IV) Complexes Against PC3 and HepG2 Cancer Cell Lines

Abedalhusaeen R. Al-Ameertaha* and Rafid H. Al-Asadi

Department of Chemistry, College of Education for Pure Sciences, University of Basrah, Basrah, 61004, Iraq

ARTICLE INFO

ABSTRACT

Thiourea derivatives have attracted attention for their pharmaceutical potential due to their diverse biological activities, including anticancer properties against various cancer types. The present study focused on the synthesis, characterization, and anticancer evaluation of thiourea benzamide derivatives and their Cu(II) and Pt(IV) complexes against human prostate cancer (PC3) and human liver cancer (HepG2) cell lines. Two thiourea benzamide ligands, N-([4-chlorophenyl]carbamothioyl)-4-fluorobenzamide (L1) and N-([4-chlorophenyl]carbamothioyl)-4-methoxybenzamide (L2) were synthesized through nucleophilic substitution reactions. Their corresponding copper and platinum complexes were also prepared and characterized. *In vitro* cytotoxicity was evaluated against PC3 and HepG2 cancer cell lines using the MTT (3-[4,5-dimethylthiazol-2-yl]-2,5-diphenyltetrazolium bromide) assay. Molecular docking studies were performed to assess binding affinities to cancer-related proteins. Computational analyses, using density functional theory (DFT) were conducted to provide theoretical insights into the geometrical structures. The synthesis of thiourea benzamide derivatives and their Cu(II) and Pt(IV) complexes resulted in several structurally characterized compounds with distinct spectral properties. Anticancer evaluations revealed that the Cu-based complex ([Cu(L2)$_2$].2H$_2$O) exhibited moderate activity against PC3 and HepG2 cell lines and the Pt-based complex ([Pt(L2)$_2$Cl$_2$].H$_2$O) demonstrated significantly lower efficacy against PC3 but showed promising effects against HepG2. Molecular docking indicated stronger interactions of the Pt complex with target proteins, highlighting its potential as a more effective inhibitor than the ligands and Cu complex. These findings underscore the therapeutic potential of thiourea derivatives and their metal complexes in anticancer drug development, suggesting further exploration into their mechanism of action and application in targeted therapies.

Keywords: Benzoyl Thiourea, Molecular docking, Prostate cancer, Metal complexes, Liver cancer

Introduction

Thioureas are excellent chemical compounds in organic chemistry and organic synthesis. They are the basis for many pharmaceutical and bioactive materials with therapeutic and medicinal properties.[1] The presence of two active primary amine groups makes thiourea a suitable starting material for synthesizing numerous derivatives. The compound provides several applications in the different fields of the pharmaceutical industry due to its biological activities. These activities include anti-parasitic and anticancer properties, where various types of cancer can be treated if diagnosed in the early stage.[2] Thiourea derivatives are particularly effective in cases of breast, prostate, and lung cancer.[3] They also exhibit anti-tuberculosis,[4] antimicrobial, and analgesic properties.[5] Benzoyl thiourea derivatives are known for their broad antioxidant, antifungal, antibacterial,[6] antitumour,[7] anti-inflammatory, and antidiabetic,[8] activities.

*Corresponding author. E mail: abedalhusaeen198082@gmail.com
Tel: +69647705646999

Thiourea derivatives also function as anticoagulants by inhibiting the arachidonic acid pathway in human blood platelets, reducing the production of prostaglandin E2 (PGE2) and thromboxane B2 (TXB2).[9] Additionally, they have demonstrated efficacy against several DNA and RNA-related viruses,[10] including antidepressant, antiallergic, and antiepileptic activities.[11] Thiourea derivatives have also been used as herbicides, antioxidant, antibacterial, antifungal, anti-tuberculosis, antispasmodic, anti-HIV, anti-inflammatory, antimalarial, antimicrobial, and antitumour agents.[12] They also exhibit insecticidal activity,[13] and serve as chelating ligands to remove heavy metal pollutants, forming stable complexes with heavy metal ions. Thiourea has been employed as a corrosion inhibitor to extract various metal ions, exhibiting distinct properties different from urea due to the difference in electronegativity between sulfur and oxygen atoms.[14] The compound exhibits higher acidity than urea and a stronger hydrogen bond donor. It is typically less soluble in water than urea.[15]

Thiourea contains three diverse functional groups: imino, thiol, and amine. The presence of two NH$_2$ groups on either side of C=S contributes to the availability of many thiourea derivatives.[16] One of the most prevalent thiourea derivatives is carbonyl thiourea, which is known as a derivative of thiourea. The simplest derivative of carbonyl thiourea, 1-ethyl thiourea (CH$_3$C(O)NHC(S)NH$_2$), was synthesized by Neuki.[17] Many transition metals, especially copper, can form stable complexes with carbonyl thiourea derivatives. They contain two strong donating groups: carbonyl and thiourea, providing both hard and soft donor sites for metal binding through nitrogen (N), oxygen (O), and sulfur (S) atoms.[18] The ability of carbonyl thiourea to effectively bind anions is attributed to the presence of two imine groups (-NH) on both the urea and thiourea moieties.

9050

This structural feature enables carbonyl thiourea to mimic the natural binding processes occurring in living cells. The thiocarbonyl groups (C=S) present in carbonyl thiourea can elevate the acidity of the compound, thereby facilitating the binding of anions compared to the analogous compound containing a carbonyl group (C=O). The compounds containing the thiocarbonyl groups lead to stability because of the formation of internal hydrogen bonds and intermolecular interactions.[19] The sulfur (S), nitrogen (N), and oxygen (O) atoms in carbonyl thiourea function as soft and hard bases, making them essential for coordinating with metal ions.[20,21]

The present study aimed to synthesize, characterize, and evaluate the anticancer potential of benzoyl thiourea derivatives and their metal complexes with copper (II) and platinum (IV) using experimental and theoretical procedures.

Materials and Methods

Sources of reagents and solvents
All reagents and solvents for synthesis and analysis were purchased commercially and used without further purification. Acetone, ethanol, 4-chlorobenzoyl chloride, 4-methoxybenzoyl chloride, 4-chloroaniline, dimethyl sulfoxide (DMSO), potassium thiocyanate, copper (II) nitrate hexahydrate, copper (II) nitrate hexahydrate, potassium hexachloroplatinate (IV), and methanol were all supplied by Sigma-Aldrich Chemicals and Merck Chemicals. All chemicals were of a high degree of purity (~97-99 %).

Instrumentation
Melting points were determined using a Thermo Scientific 9100 instrument. Infrared spectroscopy, proton nuclear magnetic resonance (^{1}HNMR), carbon-13 nuclear magnetic resonance (^{13}CNMR), and mass spectra of the ligands were recorded using a Shimadzu FTIR-84005, Bruker INSTRUM AVANCE NEO 400, and an Agilent Technologies 5975C EI-MS instrument with a power of 70 eV, respectively. ESI-MS was used to analyze the complexes quantitatively on a SHIMADZU LCMS 2010A instrument. The molar conductivity of the metal complexes was evaluated using a Cond 3110 set1, WTW, Germany instrument with a platinum electrode, with a cell constant of 1.1 cm and a concentration of 1×10^{-4} M in DMSO. Magnetic susceptibility of complexes was recorded using an Auto Magnetic Susceptibility Balance from Sherwood Company. Thermogravimetric analysis (TGA; Build 20 SDT Q600 V20.9 instrument) was carried out, with a constant rate of 20C°/min up to 800 C°. Scanning electron microscopy (SEM) measurements were performed using a Sigma VP Model-ZEISS Company FESEM instrument to visualize the particle size of the prepared compounds. X-ray diffraction (XRD) analysis was carried out with a D8 Discovery-Bruker Company XRD instrument at room temperature, with a voltage of 40 kV, a current of 40 A (1600 watts), a scanning speed of 0.01° 2θ, and an angle of 10 to 80°. The Inductively Coupled Plasma (ICP) method was used to determine the elemental ratios of the complexes using the ICP-OES-Thermo Fisher Scientific apparatus. Thin-layer chromatography (TLC) was used to check the purity and stability of the base compound.

Synthesis of the ligands and complexes
Synthesis of N-([4-chlorophenyl] carbamothioyl)-4-fluoro benzamide (L1)
A solution of 4-fluorobenzoyl chloride (10 mmol, 1.47 mL) was added gradually to a solution of potassium thiocyanate (10 mmol, 0.971 g) in 10 mL of acetone. The resulting mixture was refluxed under stirring for 1 hour. The hot filtrate was added to a solution of 4-chloroaniline (10 mmol, 1.275 g) in 20 mL of acetone. This mixture was refluxed under stirring for 1-2 hours. The TLC was used to evaluate the progress of the reaction to the end. The absolute ethanol was used as a solvent to recrystallize the obtained product. The final product was isolated as a white solid and used for further reaction. (Yield: 74.1%), M.P 205-208C°, IR spectra (KBr, cm^{-1}): 3251 (N-H), 3107, 3020 (Ar-CH), 1670 (C = O), 1602,1408 (C = C), 1263 (C-N), 1346(C=S). ^{1}HNMR (400 MHz, DMSO-d_6, δ, ppm): 1.72 (s,1H,H5),12.53(s, 1H,H6), 7.48(d,2H,H1, *J* = 8.6), 7.72(d,2H,H2, *J* = 8.3),8.07 (dd,2H,H3, *J* = 8.5, 5.4), 7.38(t, 2H,H4, *J* = 8.8 Hz), ^{13}C NMR (400 MHz, DMSO-d$_6$, δ,

ppm): 179.80 (C10), 167.56(C9), (166.69-115.88) aromatic rings. MS (EI, m/z): 308.76 [M$^+$, 19], high basis (C$_7$H$_4$FO$^+$). UV–Vis λmax/nm (ε/L.mol^{-1}.cm^{-1}): (π→π*265(7150), 310(7130), n→π*375 (40).

Synthesis of N-([4-chlorophenyl carbamothioyl]-4-methoxy benzamide (L2)
The L2 ligand was synthesized following the procedure outlined for the preparation of L1. (Yield: 54.12 %). The precipitated product was isolated as a yellow light solid. M.P: 198-200 C°. IR spectra (KBr, cm^{-1}): 3390(N-H), 3091.3028(Ar-CH), 1664(C=O), 1593.1443(C=C), 2976, 2839 C-H (Al), 1251 C-N 1344 (C=S). ^{1}H NMR (400 MHz, DMSO-d_6, δ, ppm): 11.46(S,1H,H5), 12.72(S,1H,H6) , 7.47(D,2H,H1, *J*=8.3Hz), 7.73(d,2). H, H2, *J* = 8.3), 8.03 (d, 2H, H3, *J* = 12), 7.07 (d, 2H, H4, *J* = 12), 3.86 (S, 3H, 12). H7)), ^{13}C NMR (400 MHz, DMSO-d$_6$, δ, ppm): 179.95 (C10), 167.95 (C9), (137.48-114.28), aromatic ring 56.07 (C11). MS (EI, m/z): 320.79 [M$^+$, 18], high basis (C$_7$H$_4$ClO$^+$). UV–Vis λmax/nm (ε/L.mol^{-1}.cm^{-1}): (π → π* 291 (20680), n→ π*391 (100).

Synthesis of copper (II) complexes
The prepared ligand (2 mmol, L1/L2) was added to a hot mixture of Cu(NO$_3$)$_2$.6H$_2$O (0.295 g, 1 mmol) in 20 ml of mixed solvent (1:1, MeOH: acetone). The mixture was left to reflux under stirring for 3 h. Finally, the product was precipitated by filtering the cooled mixture and washed several times with distilled water, ethanol, and diethyl ether. The resultant product was dried under a vacuum to produce the final-coloured solids.
[Cu(L1)$_2$].3H$_2$O: Dark olive colour. Yield: 63 %, M.P: 203-205 C°. IR spectrum (KBr, cm^{-1}): 3483 (O– H), 3252 (N–H), 3091 (Ar–CH), 1651 (C=O), 1600-1477 (C=C), 1271 C-N, 1309 (C=S), 850 (M-O) and 498(M-S). μ$_{eff}$ (B.M): 1.39. Molar conductivity (DMSO, Ohm^{-1}cm2mol^{-1}): 17.70. MS (ESI, m/z):733 [M+, 6], Base Peak (C$_{14}$H$_{10}$ClFN$_2$S$^+$), 292.8.
[Cu(L2)$_2$].2H$_2$O: light green. Yield: 76 %, M.P: >300C°, IR spectrum (KBr, cm^{-1}): 3387 (O– H), 3217 (N–H), 3159 (Ar–CH), 1651 (C=O), 1593-1483 (C=C), 1257 (C-N) and 1313 (C=S), 829 (M-O), 509 (M-S) μ$_{eff}$ (B.M): 1.41. Molar conductivity (DMSO, Ohm^{-1}cm2mol^{-1}): 17.16. MS (ESI, m/z): 739 [M$^+$, 8], Base Peak (C$_{15}$H$_{14}$ClN$_2$OS$^-$), 305.

Platinum (IV) complexes
The Pt-based complex was synthesized following the procedure for Cu-based complexes, with 0.486 g of K$_2$PtCl$_6$·6H$_2$O substituted.
[Pt(L1)$_2$Cl$_2$]: Dark yellow. Yield: 63 %, M.P: 253-255 C°. IR spectrum (KBr, cm^{-1}): 3375 (O– H), 3225 (N–H), 3028 (Ar–CH), 1650 (C=O), 1591-1492 (C=C), 1263 (C-N), 1321 (C=S), 847 (M-O) and 502(M-S). μ$_{eff}$(B.M): 0.00Di. Molar conductivity (DMSO, Ohm^{-1}cm2mol^{-1}): 26.5. MS (ESI, m/z): 810 [M+, 9], Base Peak (C$_{14}$H$_{10}$ClFN$_2$S$^+$), 292.8.
[Pt(L2)$_2$Cl$_2$].H$_2$O: Dark yellow. Yield: 56 %, M.P 293-295 °C. IR spectrum (KBr, cm^{-1}): 3387 (O– H), 3205 (N–H), 3115(Ar–CH), 1665 (C=O), 1599-1406 (C=C), 1256 C-N and 1321(C=S), 856 (M-O), 509 (M-S), μ$_{eff}$ =0. Molar conductivity (DMSO, Ohm^{-1}cm2mol^{-1}): 18.92. MS (ESI m/z):932 [M$^+$, 9], Base Peak (C$_{15}$H$_{14}$ClN$_2$OS$^-$), 303.

Cytotoxicity testing of the synthesized compounds using the MTT assay
The *in vitro* cytotoxicity of the test compounds was evaluated using human prostate cancer (PC3) and human hepatocarcinoma (HepG2) cell lines, which were obtained from the National Cell Bank of Iran (Institute Pasteur, Iran). The cells were supplemented with 10% fetal bovine serum (FBS; Gibco) and antibiotics (100 U/ml penicillin and 100 μg/ml streptomycin; Gibco). The cells were maintained at 37ºC and in a humidified environment with at least 5% of CO$_2$ in the air. The culture media and conditions used for growing cells as 3D colonies were identical to those used for monolayer cell culture.[22] The synthesized compounds were tested against the PC3 (a human prostate cancer cell line) and HepG2 (a human hepatocarcinoma cell line). The MTT (3-[4,5-dimethylthiazol-2-yl]-2,5-diphenyltetrazolium bromide) assay was employed to determine the inhibitory efficacy of the test compounds at various concentrations (31.25, 62.5, 125, 250, and 500 μg/mL) to obtain the IC$_{50}$ values and conducted according to the method described by Van Meerloo *et al*. (2011).[23] The cancer cell lines were treated with the various concentrations of the test compounds, while the

cells treated with the media served as the controls, representing 100% viable cells. The absorbance of the treated cells was expressed as a percentage decrease in viability compared to the controls. Origin 6.0 was used to generate graphs to obtain the IC_{50} values.

Computational study on the test compounds

The theoretical parameters were calculated using the density functional theory (DFT) method at the B3LYP level with the 6-31G (d,p) basis set (by Gaussian 09W). Moreover, to compute and depict the geometric optimization, the Gauss View 5.0 program was employed. The following equations (1-9) were used to obtain the parameters for the quantum chemical calculations.

$$\text{Energy gap } (\Delta E) = E_{LUMO} - E_{HOMO} \quad (1)$$

$$\text{Chemical hardness } (\eta) = -\frac{E_{LUMO} - E_{HOMO}}{2} \quad (2)$$

$$\text{Ionization potential } (I) = -E_{HOMO} \quad (3)$$

$$\text{Chemical softness } (\sigma) = -\frac{1}{\eta} \quad (4)$$

$$\text{Electronegativity } (A) = -E_{LUMO} \quad (5)$$

$$\text{Global softness } (S) = -\frac{1}{2\eta} \quad (6)$$

$$\text{Electronegativity } (\chi) = \frac{(E_{LUMO} + E_{HOMO})}{2} \quad (7)$$

$$\text{Global electrophilicity } (\omega) = \frac{\mu^2}{2\eta} = \frac{(-x)^2}{2\eta} \quad (8)$$

$$\text{Chemical potential } (\mu) = \frac{-(I+A)}{2} \quad (9)$$

Where E_{LUMO}: Energy of the Lowest Unoccupied Molecular Orbital; E_{HOMO}: Energy of the Highest Occupied Molecular Orbital

Molecular docking analysis

A molecular docking study was performed using MOE 2022.2. The protein crystal structure was obtained from the Protein Data Bank (PDB) (https://www.rcsb.org/structure).

Statistical analysis

The absorbance data obtained from the MTT viability experiment were analyzed using Microsoft Excel (Office Excel, 2010) to calculate the mean and standard deviation values. An average of triplicate readings from 5 wells was taken for each parameter. The statistical significance differences between the treated cells and controls were computed using Student's t-test. Significance was attributed to all p-values that were less than 0.001. The results from the DRAQ7 assay were analyzed using Microsoft Excel. The mean value for each concentration was calculated and compared to the negative control (untreated cell sample), representing 100% cell viability. The dose-response curve generated was used to estimate the IC_{50} value for each cell type examined.

Results and Discussion

Structural diagrams for the prepared organic compound and corresponding Cu-based and Pt-based complexes are depicted in Scheme 1. As demonstrated, the effect of the ligands' substituent nature (electron-donating and electron-withdrawing) and their interaction with different metal-based complexes was investigated experimentally and theoretically. The reaction between potassium thiocyanate and benzoyl chloride derivatives, conducted at a 1:1 mole ratio, yielded the corresponding benzoyl isothiocyanate (Scheme 1ia). At the same time, thiourea benzamide derivative ligands (L2 and L5) were obtained by the reaction between the products from the first step and 4-chlorophenol at a 1:1 mole ratio (Scheme 1ib). In the final step, the Cu/Pt-based complexes ([Cu(L1)₂].3H₂O, [Cu(L2)₂].2H₂O and [Pt(L1)₂Cl₂], [Pt(L2)₂Cl₂].H₂O, respectively) of the resulting ligand were synthesized using a 1:2 molar ratio of metal to the ligand in a mixed solvent (Scheme 1iia and 1iib).

Structural characteristics of the synthesized compounds

Mass spectrometry analysis showed the expected molecular ion peaks at m/z 308.1 and 320.1, corresponding to L2 and L5, respectively. These peaks, with relative abundances matching the molecular weights of the compounds, align with the molecular formulas $[C_{14}H_{10}ClFN_2OS]^+$ and $[C_{15}H_{13}ClN_2O_2S]^+$, respectively. ESI-MS spectra of complexes revealed molecular ion peaks at 733, 739, 810,

and 994, which corresponded to the molecular formula of the prepared complexes ([Cu(L1)₂].3H₂O, [Cu(L2)₂].2H₂O, [Pt(L1)₂Cl₂], and [Pt(L2)₂Cl₂].H₂O, respectively).
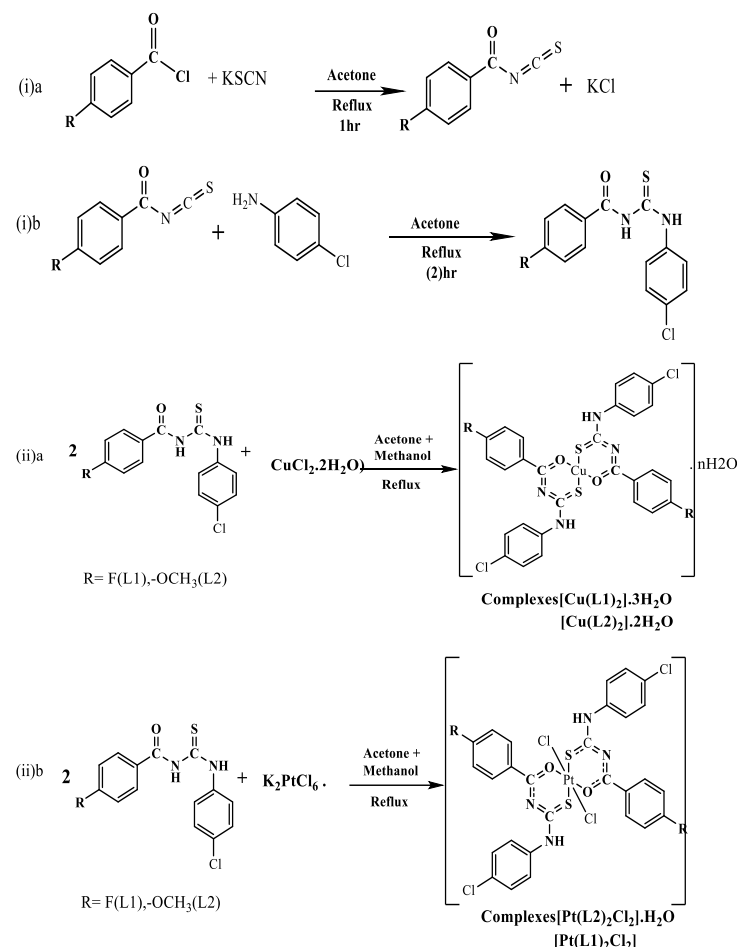
Scheme 1: Synthesis of ligands and complexes

In the FTIR spectra of L1 and L2 a distinct peak in the range of 3205–3390 cm⁻¹ was observed, corresponding to the stretching vibration of the (N-H) group, confirming the formation of the ligands. Observed peaks between 3020–3195 cm⁻¹ can be ascribed to symmetrical and asymmetrical stretching vibration of aromatic C-H for both ligands and complexes. Furthermore, the strong peak at the range 1650–1670 cm⁻¹ is attributed to the stretching vibration of the carbonyl group (C=O). This band explained the coordination between metal and ligand by shifting the initial peak related to the carbonyl group. A medium intensity band at 1406–1602 cm⁻¹ regions indicates the stretching vibration of the (C=C) group of the aromatic structure. The peaks observed in the range of 1309–1346 cm⁻¹, corresponding to the C=S group, confirm the formation of the ligands. Upon metal coordination with the ligand, the peak shift, and its intensity decreased, providing evidence of the involvement of the C=S group in the coordination.

The results of the ¹HNMR spectra demonstrated different types of signals in the range of 7.07-8.07 ppm due to the protons of the aromatic rings. The singlet signals observed at 11.72 and 11.46 ppm for L1and L2, respectively, confirm the presence of the amide group (-NH). Moreover, the (-NH) group's proton signal related to the resultant ligands appeared as a singlet peak at 12.53 and 12.72 ppm. However, the spectra of L2 exhibited a singlet peak at 3.86 ppm, which could be attributed to the presence of (O-CH₃) protons in the final compounds. Some peaks of the ¹³CNMR spectra were observed at the range 167.56 and 167.95, as well as 179.8 and 179.95 ppm, which correspond to the carbons of the C=S group inL1 and L2, respectively. However, the signals at 167.56 and 167.95 ppm were assigned to the carbon of

the carbonyl group (C=O) for L1 and L2. The aromatic carbons were manifested in the range of 114.28-166.9 ppm. However, the corresponding peak related to the aliphatic carbons appeared at 56.07 ppm in the spectra of L2. However, all the data presented using ^{1}H-NMR and IR spectra were detected by mass spectroscopy.

The molar conductivity of the synthesized compounds
The molar conductivity values of complexes (Table 1) were between 17.16 and 26.56 $Ohm^{-1}cm^2mol^{-1}$, which confirms that they did not contain counter ions with non-electrolyte properties.[24,25]

Table 1: Values of magnetic susceptibility of complexes

Chemical Formula	-(D X10^{-6})	X_g $10^{-6}\times$	X_M $10^{-3}\times$	X_A $10^{-4}\times$	μ_{eff} B.M	N electron	Geometry
[Cu(L1)$_2$].3H$_2$O	400.24	1.50	1.21	8.10	1.39	1	sp^3
[Cu(L2)$_2$].2H$_2$O	410.60	1.53	1.24	8.34	1.41	1	sp^3
[Pt(L1)$_2$ Cl$_2$]	390.62	0.00	0.00	0.3906	0.00	0	d^{2}sp^3
Pt(L2)$_2$Cl$_2$].H$_2$O]	424.60	0.00	0.00	0.2426	0.00	0	d^{2}sp^3

Magnetic properties of the synthesized complexes.
The count for the effective magnetic moment (μ_{eff}) of the copper complexes [Cu(L1)$_2$].3H$_2$O and [Cu(L2)$_2$].2H$_2$O were 1.39 and 1.41 B.M, respectively. These data confirm that the complexes containing unpaired electrons in electron configuration showed paramagnetic properties, [Ar]3d^{9}4s^{0}4p^0. The decrease in the effective magnetic moment (μ_{eff}) could be attributed to the maybe Due to the near of Cu-nuclei or formation of dimer complexes..[26] However, this observed reduction in magnetic moment can also arise due to electron delocalization or decreased ligand field symmetry.[27] Therefore, the expected geometric shape is tetrahedral (four-sided), and the hybridization type is sp3 for all copper complexes. For platinum complexes (Table 2), the electronic configuration of Pt(IV) is [Ar]4f^{14} 6S^0 5d^6, indicating a d^6 system with a low-spin configuration. Thus, the actual electron configuration for this system is (t$_2$g^6 eg^0). These complexes possess diamagnetic properties due to the absence of unpaired electrons. Based on this, it can be expected that the geometric shape of these complexes is octahedral, and the hybridization is d^{2}sp^3

Characteristics of the ligands based on ultraviolet-visible analysis
The results of the characterization of the ligands showed two distinct UV-Vis peaks. The first absorption region occurred at 265–310 *nm*, exhibiting strong peaks. However, the second absorption occurred at 375-391 nm. The molar absorption coefficients for the first and

second regions ranged from 7150-20680 L·mol^{-1}·cm^{-1} and 40-100 L·mol^{-1}·cm^{-1}, respectively. These strong absorption peaks could be attributed to π-π* electronic transitions resulting from double bonds in the aromatic rings and functional groups, such as (C=S) and (C=O). However, the absorption in the second region is relatively weaker, attributable to n-π* electronic transitions resulting from lone pairs of oxygen (O) and sulfur (S) atoms leading to the formation of electron-rich regions.

Characteristics of the synthesized complexes based on thermogravimetric analysis
The thermal decomposition of the prepared complexes was examined at high temperatures using TGA. As indicated, the multi-stage weight loss during thermal decomposition refers to the presence of crystallization area within the structure of complexes, which decomposed in the early stage of thermal disintegration at a range of 55-150 C°.[28] The second decomposition step involved removing the chloride group (Cl) and part of the ligand, occurring within a temperature range of 120–390 C°. The third stage of thermal decomposition involved further structural degradation of the ligand. As shown in Table 3, the prepared Cu-based complexes exhibited the fastest and most significant degradation and weight loss. Meanwhile, the complex prepared by Pt metal ([Pt(L2)$_2$Cl$_2$].H$_2$O) exhibited the highest residual mass value (char yield) at 800 C°.

**Table 2:** Molar conductivity values for complexes

Chemical Fotmula	Electrical conductiv Ohm^{-1}	Qualitative conductivity Ohm^{-1})	Molar conductivity Ohm^{-1}.cm-^{2}/M))	Electrical Type	Geometry
[Cu(L1)$_2$].3H$_2$O	16.0	17.70 X10^{-6}	17.70	Non electrolytic	sp^3
[Cu(L2)$_2$].2H$_2$O	15.6	17.16 X10^{-6}	17.16	Non-electrolytic	sp^3
[Pt(L1)$_2$ Cl$_2$]	24.15	26.565 X10^{-6}	26.565	Non-electrolytic	d^{2}sp^3
[Pt(L2)$_2$ Cl$_2$].H$_2$O	17.20	18.92 X10^{-6}	18.92	Non-electrolytic	d^{2}sp

Characteristics of the synthesized compounds based on scanning electron microscopy and energy-dispersive X-ray spectroscopy
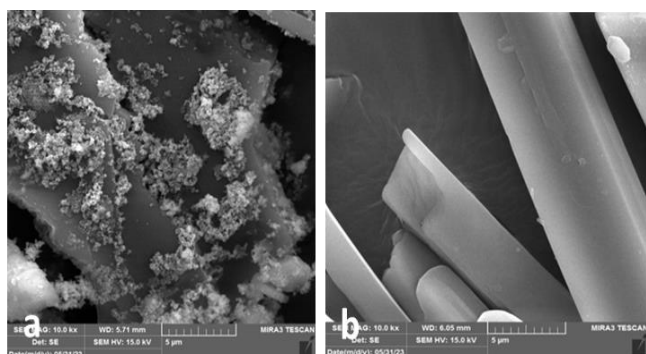Scanning electron microscopy images were utilized to examine the impact of metal coordination on the surface morphology of the

prepared compounds.[29] Energy-dispersive X-ray analysis provides information about the chemical composition of samples, including the identification and quantification of the prepared samples. It can also be

used to determine the concentrations and distribution of metals in complex compounds.[30] As observed from SEM measurements, there is a uniform morphology with a specific shape (rod-like) for all the prepared bonds (Figures 1 and 2). However, coordination of the metal with the ligand would cause changes in the surface of the molecules and the appearance of an irregular conformation.[31] Energy-dispersive X-ray (EDX) spectra of ligands and corresponding complexes with Cu are shown in Figures 3 and 4. The data confirmed that the obtained samples are pure, containing only the Cu element and the other specified elements in the final complexes (Figures 3a and 4a compared to Figures 3b and 4b).
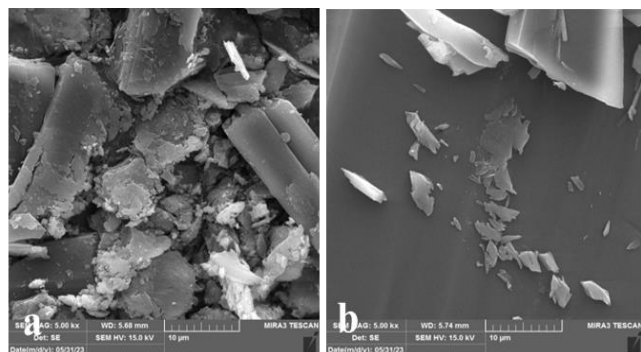
Figure 1: Scanning electron microscopy image of (a)L1 ligand particles and (b) complex [Cu(L2)$_2$].3H$_2$O particles

Figure 2: Scanning electron microscopy image of (a) L2 ligand particles and (b) complex [CuL2)$_2$].3H$_2$O particles.

Characteristics of the synthesized compounds based on X-ray diffraction analysis
The X-ray diffraction patterns provide important structural information about the microcrystalline nature of particular materials. The crystallographic structure of the obtained and the Cu-based complexes

was determined by X-ray diffraction details (Table 4). As observed, the interplanar spacing (d, Å) and relative intensities (I/I$_0$) of the ligands and their corresponding metal complexes exhibited distinct formations. The crystalline characteristics were observed in XRD patterns of resultant ligands (L1, L2). However, incorporating water molecules during the formation of the Cu(II) and Pt(IV) complexes imparts a semi-crystalline nature to the structure.[32] The absence of contaminants was confirmed by analysis of the diffraction pattern of the starting materials. The θ and d values (average volume of crystal and the size of normal to the diffraction plane, respectively), as well as the Full Width at Half Maximum (FWHM), the relative intensity (%), and the particle size, are presented in Table 4. The crystal size was calculated from the XRD patterns using the Debye-Scherrer equation.

$$B = 0.94\lambda/(S \cos \theta) \text{ --------- (10)}$$

Where S is the crystal size, θ is the diffraction angle, B is the line width at the highest half, and λ is 1.5406 Å. The d-spacing was determined using the Bragg equation:[33]
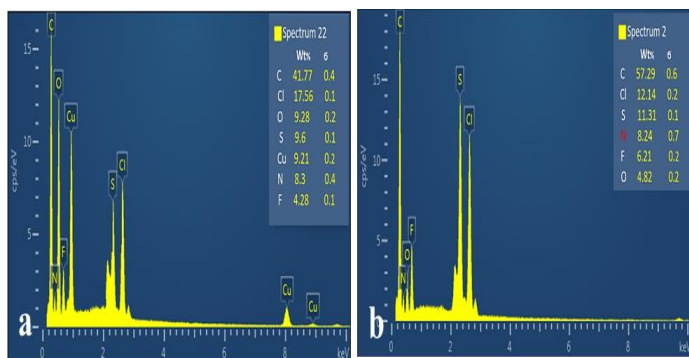
$$n\lambda = 2d \sin(\theta) \text{ at } n = 1 \text{ --------- (11)}$$

*Anticancer activity of the synthesized compounds*
Five different concentrations of compounds were used to evaluate the toxicity of synthesized compounds against PC3 and HepG2 cancer cell lines. The inhibition efficacy and the IC$_{50}$ value (concentration for half-maximal effect) were calculated. The prepared ligands with different chemical structures showed multiple efficacies against the cancer cells. This was evident from the IC$_{50}$ values (Table 5). Reactive species, such as oxygen, nitrogen, and sulfur can inhibit important enzymes necessary for tumour growth.[34,35] As presented in Table 5, the Cu-based complex ([Cu(L2)$_2$].2H$_2$O) exhibited moderate activity, while the Pt-based complex ([Pt(L2)$_2$Cl$_2$].H$_2$O) demonstrated significantly lower activity against PC3. However, Pt-based complex ([Pt(L2)$_2$Cl$_2$].H$_2$O) exhibited significant effects against Cu-based complex ([Cu(L2)$_2$].2H$_2$O), which has a moderate interaction with HepG2. Nevertheless, the ligands are not very effective against cancer cells. Multiple studies have demonstrated that the complexes exhibit significantly greater effectiveness in permeating cancer cell membranes compared to the free ligand.[36] Average concentration values were calculated and compared to the negative control (untreated cell sample), representing 100% cell viability.

Table 3: Thermogravimetric analysis (TGA) data of the complexes

Complex	Stapes	Temp. range	Decomposition parts	weight loss %	
				Calculated	Found
[Cu(L1)$_2$].3H$_2$O	1	47-158	3H$_2$O	7.36	7.47
(M.wt=733g/mol)	2	158-285	2(C$_8$H$_7$FN)+2Cl	46.79	47.18
	3	285-389	C$_5$H$_8$	10.64	9.29
	4	380-800	C$_6$H$_7$N	12.55	11.80
	Remaining		CuH$_4$O$_2$S$_2$	22.66	24.25
	1	50-151	2H$_2$O	4.87	4.90
[Cu(L2)$_2$].2H$_2$O	2	151-280	2(C$_6$H$_5$Cl)+2(C$_7$H$_8$O)	59.50	58.00
(M.wt=739/mol)	3	280-445	2(CH$_4$N$_2$)	11.90	11.30
	4	445-800	2(CH3)+2S	12.70	12.12
	Remaining		CuH$_2$O$_2$	13.12	13.80
[Pt(L1)$_2$Cl$_2$]	1	70-370	2(C$_6$H$_7$N)+(C$_6$H$_6$)+4Cl+F	50.62	50.93
(M.wt=881g/mol)	2	370-800	(C$_8$H$_8$NS)+CH$_3$NS	23.9	22.48
	Remaining		CH$_3$O$_2$Pt	27.4	26.59
[Pt(L2)$_2$Cl$_2$].H$_2$O	1	55-120	H$_2$O	1.95	2.280
(M.wt=932g/mol)	2	120-335	2Cl+CH$_3$	10.8	12.44
	3	335-496	C$_6$H$_6$O	10.0	9.843
	4	496-660	C$_6$H$_6$O	10.0	9.22
	5	660-800	Cl	3.8	2.592
	Remaining		C$_{16}$H$_{13}$ClN$_4$O$_2$PtS$_2$	62.9	63.62

Figure 3: Energy-dispersive X-ray (EDX) spectrum of (a) ligandL1and (b) [Cu(L1)$_2$].3H$_2$O complex.
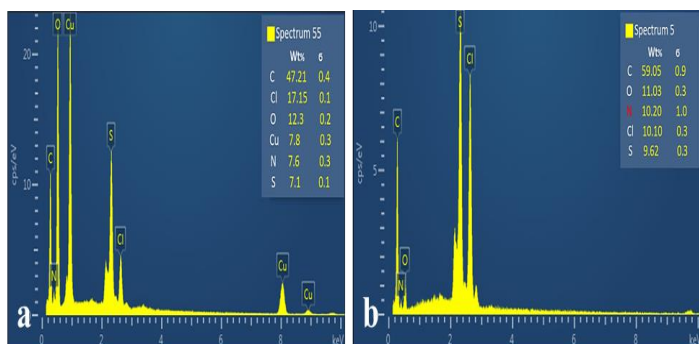
**Figure 4**: Energy-dispersive X-ray (EDX) spectrum of (a) ligand L2 and (b) [Cu(L2)$_2$].2H$_2$O complex.

The theoretical evaluation of ligands

The results of the theoretical evaluation of ligands are presented in Figures 5 and 6, and Tables 6-9. The parameters obtained are opposing criteria for determining the number of dipoles at the molecular scale. Electronegativity is the ability of chemical species to attract electrons, a crucial parameter for determining inhibitory performance.[37] The results indicated that the L1 ligand exhibited higher electronegativity compared to the L5 ligand. These findings align with the observations made with the anticancer potential. Determination of the HOMO (π donor) and the LUMO (π acceptor) as the molecular orbital energies is crucial information for the calculation of quantum chemical. The HOMO orbital primarily functions as an electron donor, while the LUMO orbital serves as an electron acceptor. However, the values of these functions are negative amounts, which confirms the stability of the formulated compounds.[38] The energy gap (E$_{LUMO}$–E$_{HOMO}$) determines a molecule's stability and provides insight into the molecular stability during chemical reactions.[39] Therefore, by elevating the different potentials, molecules become much less active and more stable. However, molecules with small energy gaps are more easily polarized and have greater potential for chemical reactivity.[40]

As shown in **Table 6**, the resultant compounds exhibit stability, as indicated by the negative values of the E$_{HOMO}$ and E$_{LUMO}$ orbitals. The energy gap (ΔE), chemical softness (S), chemical hardness (η), and

absolute softness (σ) are related to the chemical composition of the molecules. Molecule L1 exhibited high values of ΔE and hardness (η). However, it has a lower amount for absolute softness (σ), chemical softness (S), and absolute softness (σ). Therefore, this compound is comparatively more stable than the other samples. Moreover, as depicted for compound L2, the values of chemical hardness (η), as well as the energy gap (ΔE), are lower than L1, whereas the values for the chemical softness (S) are higher compared to the analogue compound. Therefore, the ligand L2 is much more reactive than the other analogue ligand L1. Thus, different ligands can be selected based on the variations in biological conditions.[41] Compared to the compound L1 (Table 6), the L2 molecule had a higher electronegativity (χ). Thus, the findings are in agreement with the anticancer study results.

Global electrophilicity (ω) is a crucial indicator of the potential of activity for comparing the molecules and their talent to attract electrons.[42] As expected, the high global electrophilicity of the molecule suggests that the molecule acts as a magnet to absorb electrons. Orbital localization of the HOMO has been observed mainly in the fragments of sulfur, oxygen, and nitrogen atoms. The LUMO orbitals with π character are centered on the phenyl ring. Electronic maps are useful for evaluating the potential sites of electrophilic attack. The maps display electron energies and facilitate nucleophilic interactions and hydrogen bonding.[43] The electrostatic and electrostatic potential contour maps (Figure 6) indicated that the regions around the sulfur and oxygen atoms are very active due to the high density of electrons around them.
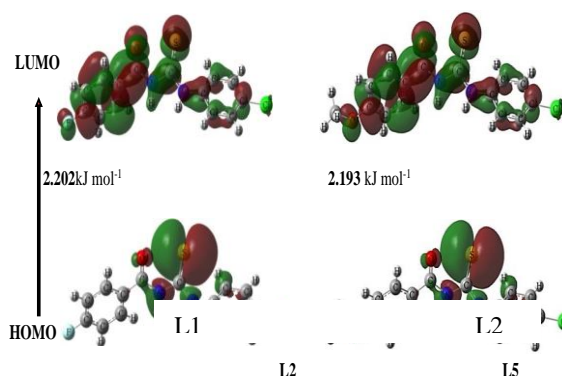
Figure 5: HOMO-LUMO constructions of the ligands.
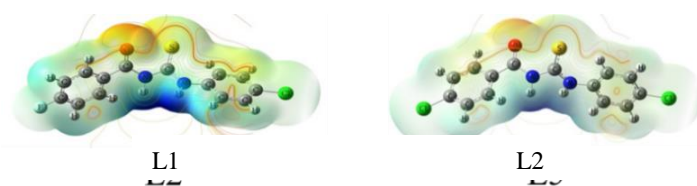
Figure 6: Electrostatic potential maps and Contour electrostatic potential around the L1 and L2 molecules.

Table 4: X-ray diffraction (XRD) spectral data of the highest intensity value for the prepared ligands and their complexes.

Compound	size of particles(nm)	θ	Height [cts]	dspacing (Å)	Full Width at Half Maximum Level
L1	10.00	15.965	6889.08	5.54657	0.150670

[Cu(L1)$_2$].3H$_2$O	2.790	5.590	2217.800	15.79692	0.521000
L2	13.670	7.2014	5370.423	12.26532	0.107180
[Cu(L2)$_2$].2H$_2$O	12.150	5.238	10312.290	16.85534	0.120170

Table 5: Anticarcinogenic activity and IC$_{50}$ values of the obtained compounds against PC3 and HepG2 cells.

Compounds	Prostate Cancer (PC3 cell line) Concentration (µg/ml)					IC$_{50}$(µg/ml)
	31.25	62.5	125	250	500	
	Cells inhibition (%)					
L1	15.60	27.00	42.83	60.97	71.65	169.51
L2	2.69	8.08	27.79	47.50	72.13	255.79
[Cu(L2)$_2$].2H$_2$O	15.76	20.49	36.39	60.32	68.62	198.25
[Pt(L2)$_2$Cl$_2$].H$_2$O	15.62	42.72	71.92	77.79	83.52	85.06
	Liver Cancer (HepG2)					
L1	23.17	32.83	46.5	49.33	71.58	173.04
L2	5.75	17.33	31.83	41.08	51.83	424.72
[Cu(L2)$_2$].2H$_2$O	36.13	43.95	57.1	75.16	80.27	76.35
[Pt(L2)$_2$Cl$_2$].H$_2$O	43.11	70.56	76.41	78.6	85.18	26.19

Table 6: Calculated parameters for the optimized structures.

Comp	E$_{HOMO}$	E$_{LUMO}$	(ΔE)	(I)	(A)	(χ)	(η)	(σ)	(S)	(µ)	(ω)
L1	-7.437	-5.235	2.202	7.437	5.235	6.336	1.101	0.908	-0.551	-6.336	18.231
L2	-7.433	-5.24	2.193	7.433	5.24	6.337	1.097	0.912	-0.548	-6.337	18.309

Characteristics of synthesized compounds based on thermodynamic parameters

Enthalpy (ΔH°), entropy (ΔS°), and free energy (ΔG°) are important parameters used to understand and describe the behaviour of thermal systems. Enthalpy measures the thermal energy in a system and indicates heat absorbed or released at constant pressure. Entropy quantifies a system's degree of disorder and energy distribution. Free energy represents the balance between enthalpy and entropy contributions and measures the energy available at constant temperature and pressure. The values of ΔH° and ΔS° were directly obtained from the output of the Gaussian program, and ΔG° was calculated using the equation ΔG° = ΔH° - TΔS°, with T = 298K. Free energy (ΔG°) is related to free electrons and nuclei. For the compounds L1 and L2, the values of ΔH° were found to be -4416764 and -4456810 kJ/mol, while the values of ΔS° were 0.630979865 and 0.617593959 kJ/mol·K, respectively. However, the values of ΔG° related to the L2 and L5 ligands were calculated as 4416943- , and -4457000 kJ/mol, respectively. It was observed that compound L1 had the lowest values of ΔG° and ΔH° and the highest value of ΔS°. This result indicated that it is thermally more stable compared to L2.

Table 7: Bonds lengths of the prepared compounds

The bond length (Å)	L1	L2	X-ray analysis
R1-C1	1.500	1.495	1.605
C1=O	1.214	1.215	1.221
C1-N1	1.405	1.409	1.376
N1-C2	1.408	1.404	1.391
C2=S	1.653	1.654	1.663
C2-N2	1.375	1.477	1.376
N2-R2	1.413	1.412	1.388

Modelling the three-dimensional (3D) structure of the prepared ligands

Molecular modelling explores structural components and offers insights into molecular behaviour. This is particularly valuable because data obtained through X-ray crystallography is scarce and challenging to acquire. The bond lengths, bond angles, and dihedral angles, essential structural parameters of the synthesized compounds, were measured

9056

and analyzed. This analysis aims to describe the physical and chemical properties of the molecules. Tables 7 and 8 compare optimized bond lengths and angles between experimental atomic positions,[44,] and theoretically calculated values, demonstrating consistency with the experimental results. Additionally, Table 9, which lists the dihedral angles, indicated that the compounds exhibit non-planar geometries. Calculating the Mulliken charges is important in understanding the nature of atoms and making quantitative predictions about experimental results.[45] Based on the Mulliken charge values, the N2 atom exhibits

the highest negative potential (greatest basicity), with values of -0.614 and -0.616, followed by N1 (-0.593 and -0.595), O (-0.452 and -0.458), and finally S (-0.160 to -0.163 and -0.170) for L1and L2 respectively.

Molecular docking outcome
A molecular docking study was conducted to analyze ligand L2, along with the complexes [Cu(L2)$_2$]·2H$_2$O and [Pt(L2)$_2$Cl$_2$]·H$_2$O, in interaction with HepG2 cell proteins.[46,47] The proteins examined were (EGFR) (PDP: 3W32).

Table 8: Triangular angles (º) of the prepared compounds

riangular Angles (º)	L1	L2	X-ray analysis
R1-C1=O	122.49	122.87	121.12
R1-C1-N1	114.12	114.08	116.14
O=C1-N	123.34	122.99	122.12
C1-N1-C2	127.64	127.87	129.09
N1-C2=S	122.52	123.77	118.26
N1-C1-N2	109.18	109.21	113.79
S=C2-N2	127.27	127.00	127.99
C2-N2-R2	131.95	131.09	133.93

Table 9: Drilateral angles (º) of the prepared compounds

Quadrilateral angle (º)	L1	L2
R1-C1-O-N1	177.30	177.14
R1-C1-N1-C2	167.43	167.62
O-C1-N1-C2	-15.04	-15.00
C1-N1-C2-N2	146.11	147.30
N1-C2-N2-R2	169.52	169.56
N1-C2-S-N2	-177.92	-178.04
S-C2-N2-R2	-8.64	-8.71

The interaction between the protein (3W32) and the complex [Pt(L2)$_2$Cl$_2$].H$_2$O was the strongest, followed by the complex [Cu(L2)$_2$].2H$_2$O and finally the ligand L2, with **RMSD** values of -10.174, -9.7268, and -7.2070, respectively (**Table 10**). The docking study was used to assess the interaction between amino acid residues and hydrogen bonds of target proteins with ligand L2 and complexes
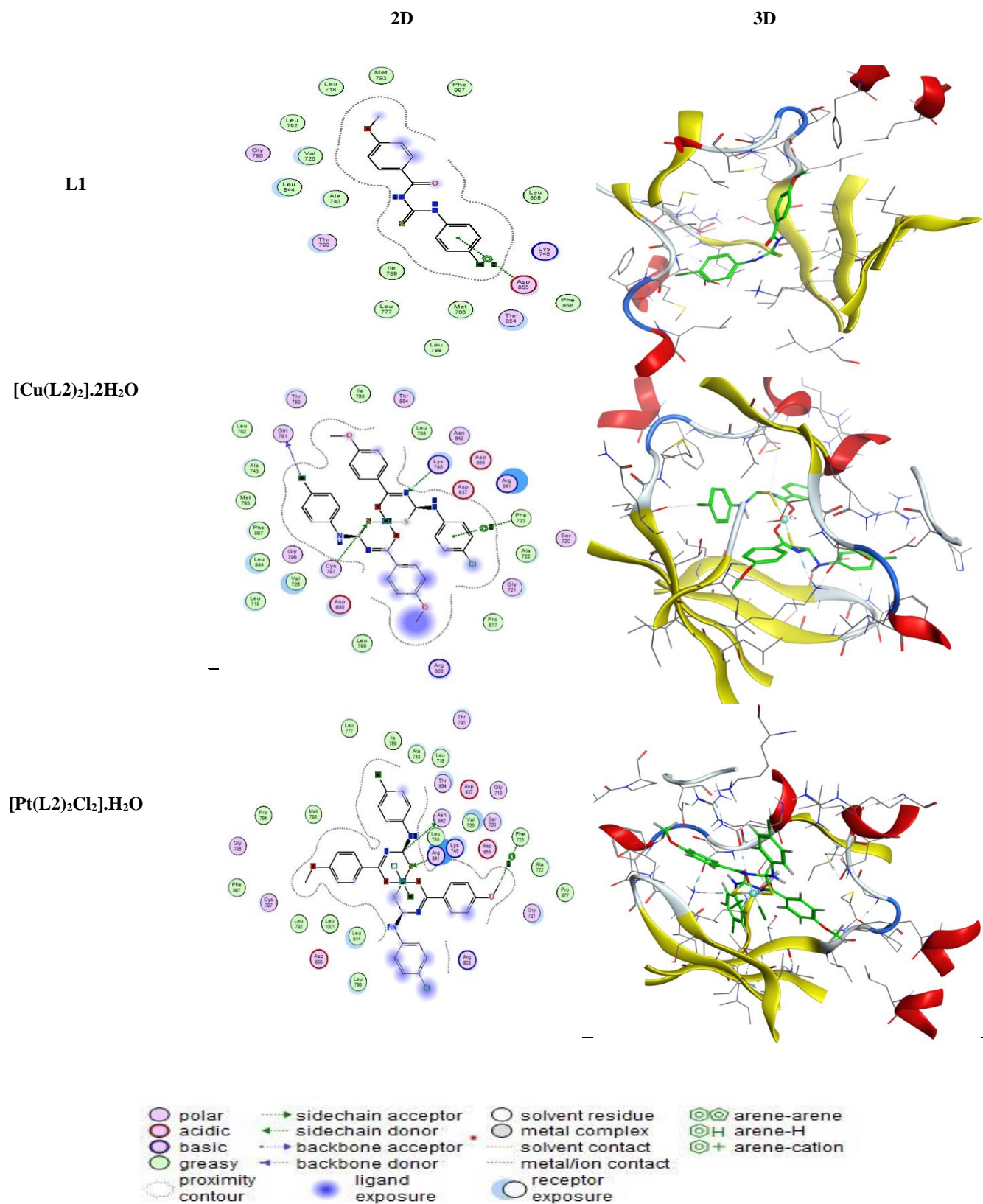
[Cu(L2)$_2$].2H$_2$O and [Pt(L2)$_2$Cl$_2$].H$_2$O. **Figure 7** displays the two-dimensional (2D) and three-dimensional (3D) structures. The results reveal three hydrogen bonds between the compound [Pt(L2)$_2$Cl$_2$].H$_2$O and the protein. Among these bonds, one acts as a donor through the C atoms, while the other acts as an acceptor through the S atom.

Table 10: Molecular docking data of compound with PDB (3W32) proteins

Compound	Binding energy (S) (kJ/mol)	RMSD (Å)	Atom of Compound	Atom of Receptor	Amino acid receptor	Type of Interaction Bond	Distance (Å)	E (Kcal/mol)
[Pt(L2)$_2$Cl$_2$].H$_2$O	-10.174	1.915	C(44)	OD1	ASN(842)	H-donor	3.30	-0.8
			S(49)	NZ	LYS(745)	H-ecceptor	3.33	-6.1
			C(64)	6-Ring	PHE(723)	H-pi	4.48	-0.5
[Cu(L2)$_2$].2H$_2$O	-9.7268	1.391	Cl(60)	O	GLN(791)	H-donor	4.0	-0.5
			N(13)	NZ	LYS(745)	H-ecceptor	3.13	-8.0
			S(49)	CB	CYS(745)	H-ecceptor	3.56	-0.5
			6-Ring	N	PHE(723)	Pi-H	4.76	-0.9
L2	-7.2070	1.950	6-Ring	N	ASP(855)	Pi-H	3.78	-0.8

At the same time, the third bond is in the form of an H-donor with an aromatic ring. [Cu(L2)$_2$].2H$_2$O formed a donor bond (H-donor) with the amino acid GLN (791) through the Cl atom and also formed two acceptor bonds (H-acceptor) with the amino acid LYS (745) through the N atom. The amino acid CYS (745) is linked by S. The last bond is of the Pi-H type with the amino acid PHE (723). For the L5 ligand, a Pi-H bond was formed with the amino acid ASP855 via the aromatic

ring. The results of molecular docking indicate that the complex [Pt(L2)$_2$Cl$_2$].H$_2$O has the lowest RMSD value, which suggests that it is the most effective inhibitory compound, followed by [Cu(L2)$_2$].2H$_2$O, then L2. These results are consistent with the study of biological effectiveness and practical inhibitory values against HepG2 cells.

Figure 7: 2D and 3D forms of ligand L5 and complexes: [Cu(L2)$_2$].2H$_2$O and [Pt(L2)$_2$Cl$_2$].H$_2$O with 3W32 protein.

Conclusion

The study revealed that the L1 and L2 ligands coordinated with Cu(II) and Pt(IV) ions act as bidentate ligands, binding through the sulfur atom of the (C=S) group and the oxygen atom of the C=O group (S1O1 coordination). The Pt(IV) complexes exhibit octahedral geometry (d^2sp^3), while the Cu(II) complexes adopt a tetrahedral geometry (sp^3). All prepared complexes demonstrated non-electrolytic behaviour and contained lattice water molecules, except for $[Pt(L1)_2Cl_2]$, which lacks water molecules. The platinum-based complexes showed greater effectiveness than copper-based complexes, whereas the ligands exhibited minimal or no activity against prostate and pancreatic cancer cells. The synthesized compounds were relatively stable, with L2 and its complexes $[Cu(L2)_2]\cdot2H_2O$ and $[Pt(L2)_2Cl_2]\cdot H_2O$ showing specificity for the 3W32 protein, a target in hepatocellular carcinoma (HepG2) cells.

Conflict of interest

The authors declare no conflict of interest.

Authors' Declaration

The authors hereby declare that the work presented in this article is original and that any liability for claims relating to the content of this article will be borne by them.

References

1. Saeed A, Mustafa MN, Zain-ul-Abideen M, Shabir G, Erben MF, Flörke U. Current developments in chemistry, coordination, structure and biological aspects of 1-(acyl/aroyl)-3-(substituted) thioureas: advances continue. J Sulfur Chem. 2019;40(3):312-350.

2. Kirishnamaline G, Magdaline JD, Chithambarathanu T, Aruldhas D, Anuf AR. Theoretical investigation of structure, anticancer activity and molecular docking of thiourea derivatives. J. Mol. Struct. 2021;1225:129118.

3. Salvador-Gil D, Herrera RP, Gimeno MC. Catalysis-free synthesis of thiazolidine--thiourea ligands for metal coordination (Au and Ag) and preliminary cytotoxic studies. Dalton Trans, 2023, 52(23): 7797-7808.

4. Karakucs S., Rollas S. Synthesis and antituberculosis activity of new N-phenyl-N′-[4-(5-alkyl/arylamino-1, 3, 4-thiadiazole-2-yl) phenyl] thioureas. Il Farmaco. 2002;57(7):577-581.

5. Shakeel A, Altaf AA, Qureshi AM, Badshah A. Thiourea derivatives in drug design and medicinal chemistry: A short review. J drug des med chem. 2016;2(1):10.

6. Singh V, Singh S, Verma A, Choudhary RR, Gupta S. Synthesis, characterization and solid state conductivity of nitro-phenol-benzaldehyde urea based ligand and trithiocarbonate. Mater. Today. Proc. 2022;51:496-501.

7. Faihan AS, Al-Jibori SA, Hatshan MR, Al-Janabi AS. Antibacterial, spectroscopic and X-ray crystallography of newly prepared heterocyclic thiourea dianion platinum (II) complexes with tertiary phosphine ligands. Polyhedron. 2022;212:115602.

8. Chen WH, Mi JX. A new redox-based approach for synthesizing a mixed-valence hybrid polymolybdate uncommonly bicapped by Cr (III) coordination complexes. Polyhedron. 2015;85:117-123.

9. Faidallah HM, Al-Mohammadi MM, Alamry KA, Khan KA. Synthesis and biological evaluation of fluoropyrazolesulfonylurea and thiourea derivatives as possible antidiabetic agents. J. Enzyme Inhib. Med. Chem. 2016;31(sup1):157-163.

10. Lourenço, A. L., Saito, M. S., Dorneles, L. E. G., Viana, G. M., Sathler, P. C., de Sequeira Aguiar, L. C., De Pádula, M., Domingos, T. F. S., Fraga, A. G. M., Rodrigues, C. R., and others. Synthesis and antiplatelet activity of antithrombotic thiourea compounds: biological and structure-activity relationship studies. Molecules. 2015;20(4):7174-7200.

11. Sanna, G., Madeddu, S., Giliberti, G., Piras, S., Struga, M., Wrzosek, M., Kubiak-Tomaszewska, G., Koziol, A. E., Savchenko, O., Lis, T., and others, Synthesis and biological evaluation of novel indole-derived thioureas. Molecules. 2018;23(10):2554.

12. Javadzade, T., Rzayeva, I., Demukhamedova, S., Akverdieva, G., Farzaliyev, V., Sujayev, A., and Chiragov, F. Synthesis, structural analysis, DFT study, antioxidant activity of metal complexes of N-substituted thiourea. Polyhedron. 2023;231:116274.

13. Zahra U, Saeed A, Fattah TA, Flörke U, Erben MF. Recent trends in chemistry, structure, and various applications of 1-acyl-3-substituted thioureas: a detailed review. RSC.advances. 2022;12(20):12710-12745.

14. Ray DA, Baniasadi M, Graves JE, Greenwood A, Farnaud S. Thiourea leaching: an update on a sustainable approach for gold recovery from E-waste. J. Sustain. Metall. 2022;8(2):597-612.

15. Raza, M. A., Javaid, K., Farwa, U., Javaid, A., Yaseen, M., Maurin, J. K., Budzianowski, A., Iqbal, B., and Ibrahim, S., One pot efficient synthesis of 1, 3-di (Naphthalen-1-yl) thiourea; X-ray structure, hirshfeld surface analysis, density functional theory, molecular docking and in-vitro biological assessment. J. Mol. Struct. 2023;1271:133989.

16. Khan E, Khan S, Gul Z, Muhammad M. Medicinal importance, coordination chemistry with selected metals (cu, Ag, au) and Chemosensing of Thiourea derivatives. A review. Crit. Rev. Anal. Chem. 2021;51(8):812-834.

17. González DLN, Saeed A, Shabir G, Flörke U, Erben MF. Conformational and crystal structure of acyl thiourea compounds: The case of the simple (2, 2-dimethyl-propionyl) thiourea derivative. J. Mol. Struct. 2020;1215:128227.

18. Al-Abbassi AA, Kayed SF, Kassim MB. Spectral, theoretical, physicochemical and corrosion inhibition studies of ortho-, meta-and para-hydroxyphenyl-benzoylthiourea ligands. Inorg. Chem. Commun. 2023;156:111155.

19. Muhammad, M., Khan, S., Shehzadi, S. A., Gul, Z., Al-Saidi, H. M., Kamran, A. W., and Alhumaydhi, F. A.. Recent advances in colorimetric and fluorescent chemosensors based on thiourea derivatives for metallic cations: A review. Dyes Pigm. 2022;205:110477.

20. Muhammed RA, Abdullah BH, Rahman HS. Synthesis, cytotoxic, antibacterial, antioxidant activities, DFT, and docking of novel complexes of Palladium (II) containing a thiourea derivative and diphosphines. J. Mol. Struct. 2024;1295:136519.

21. Swaminathan S, Jerome P, Deepak RJ, Karvembu R, Oh TH. Platinum group metal (PGM) complexes having acylthiourea ligand system as catalysts or anticancer agents. Coord. Chem. Rev. 2024;503:215620.

22. Al-Salim YM, Al-Asadi RH. Synthesis, Anti-breast Cancer Activity, and Molecular Docking Studies of Thiourea Benzamide Derivatives and Their Complexes with Copper Ion. Trop. J. Nat. Prod. Res. 2023;7(6) 510–518.

23. Van Meerloo J, Kaspers GJL, Cloos J. Cell sensitivity assays: the MTT assay. Cancer cell culture. Meth. Protoc. 2011;237–245.

24. Nawar F, Al-Asadi R, Abid D. Synthesis, antibacterial activity and DFT calculations of some Thiazolidine-4-Carboxylic acid derivatives and their complexes with Cu (II), Fe (II) and VO (II). Egypt. J. Chem. 2020;63(1):349-362.

25. El-ghamry MA, Nassir KM, Elzawawi FM, Aziz AAA, Abu-El-Wafa SM. Novel nanoparticle-size metal complexes derived from acyclovir. Spectroscopic characterization, thermal analysis, antitumour screening, and DNA cleavage, as well as

3D modeling, docking, and electrical conductivity studies. J. Mol. Struct. 2021;1235:130235.

26. Lo SMF, Chui SSY, Shek LY, et al. Solvothermal synthesis of a stable coordination polymer with copper-i copper-ii dimer units:[Cu4 {1, 4-C6H4 (COO) 2} 3 (4, 4 '-bipy) 2] n. J. Am. Chem. Soc. 2000;122(26):6293-6294.

27. El-Saied FA, El-Bahnasawy RM, Azzem MA, El-Sawaf AK. Synthesis, characterization and electrochemical properties of β-diketone complexes of ruthenium (III). Polyhedron. 1994;13(11):1781-1786.

28. Al-Daffay RKH, Al-Hamdani AAS. Synthesis and characterization of some metals complexes with new Acidicazo ligand 4-[(2-amino-4-phenylazo)-methyl]-cyclohexane carboxylic acid. Iraqi J. Sci. 2022:3264-3275.

29. Pokhrel N, Agioutanti E, Keles C, Afrouz S, Sarver E. Comparison of respirable coal mine dust constituents estimated using FTIR, TGA, and SEM-EDX. Mining. Metall. Explor. 2022;39(2):291-300.

30. Refat MS, El-Deen IM, Ibrahim HK, El-Ghool S. Synthesis and spectroscopic studies of some transition metal complexes of a novel Schiff base ligands derived from 5-phenylazo-salicyladehyde and o-amino benzoic acid. Spectrochim. Acta A. Mol. Biomol. Spectrosc. 2006;65(5):1208-1220.

31. Din, S. U., Iqbal, H., Haq, S., Ahmad, P., Khandaker, M. U., Elansary, H. O., Al-Harbi, F. F., Abdelmohsen, S. A. M., and El-Abedin, T. K. Z. Investigation of the biological applications of biosynthesized nickel oxide nanoparticles mediated by Buxus wallichiana extract. Crystals. 2022;12(2):146.

32. El-Shwiniy WH, Ibrahim AG, Sadeek SA, Zordok WA. Synthesis, structural elucidation, molecular modeling and antimicrobial studies of 6-(2-hydroxyphenylimine)-2-thioxotetrahydropyrimidin-4 (1H)-one (L) Schiff base metal complexes. Appl. Organomet. Chem. 2021;35(5):e6174.

33. Deswal, Y., Asija, S., Tufail, A., Dubey, A., Deswal, L., Kumar, N., Saroya, S., Kirar, J. S., and Gupta, N. M.. Instigating the in vitro antidiabetic activity of new tridentate Schiff base ligand appended M (II) complexes: From synthesis, structural characterization, quantum computational calculations to molecular docking, and molecular dynamics simulation studies. Appl. Organomet. Chem. 2023;37(4):e7050.

34. Abd El-Lateef HM, Ali AM, Khalaf MM, Abdou A. New iron (III), cobalt (II), nickel (II), copper (II), zinc (II) mixed-ligand complexes: Synthesis, structural, DFT, molecular docking and antimicrobial analysis. Bull. Chem. Soc. Ethiop.2024;38(1):147-166.

35. Rawat, V., Gulati, K., Kaur, U., Seth, J. K., Solanki, V., Venkatesh, A. N., Singh, D. P., Singh, N., Loganathan, M., and others,. A Supervised Learning Identification System for Prognosis of Breast Cancer. Math. Probl. Eng. 2022.1 (2022): 7459455

36. Ji, P., Wang, P., Chen, H., Xu, Y., Ge, J., Tian, Z., and Yan, Z. Potential of copper and copper compounds for anticancer applications. Pharmaceuticals. 2023;16(2):234.

37. Zahid, H., ul Ghazali, Z., Shehzad, R. A., Iqbal, J., Al-Buriahi, M. S., Alfryyan, N., Mahmoud, Z. M. M., and Alrowaili, Z. A.. Designing phenyl-di-p-tolyl-amine-based asymmetric small molecular donor materials with favorable photovoltaic parameters. Optik. 2022;256:168739.

38. Naseem, Z., Shehzad, R. A., Jabeen, S., Tahir, S., Mushtaq, F., Zahid, M., and Iqbal, J.. Quantum chemical investigation of choline chloride-based deep eutectic solvents. Chem. Phys. 2023;571:111936.

39. Barroso J, Pan S, Merino G. Structural transformations in boron clusters induced by metal doping. Chem. Soc. Rev. 2022;51(3):1098-1123.

40. Alharis R, Al-Asadi RH, Hassan DA. New Mercurated and Tellurated Sulpha Compounds: Synthesis, Invitro Anticancer Study and DFT Calculation. Egypt. J. Chem. 2021;64(10):5755-5764.

41. Kaya, S., Kaya, C., Guo, L., Kandemirli, F., Tüzün, B., U.ugurlu,.Ilkay, Madkour, L. H., and Saraço.uglu, M. Quantum chemical and molecular dynamics simulation studies on inhibition performances of some thiazole and thiadiazole derivatives against corrosion of iron. J. Mol. Liq. 2016;219:497-504.

42. Tolmachev, D., Lukasheva, N., Ramazanov, R., Nazarychev, V., Borzdun, N., Volgin, I., Andreeva, M., Glova, A., Melnikova, S., Dobrovskiy, A., and others. Computer simulations of deep eutectic solvents: Challenges, solutions, and perspectives. Int. J. Mol. Sci. 2022;23(2):645.

43. Chakraborty D, Chattaraj PK. Conceptual density functional theory based electronic structure principles. Chem. Sci. 2021;12(18):6264-6279.

44. Arshad, N., Rafiq, M., Ujan, R., Saeed, A., Farooqi, S. I., Perveen, F., Channar, P. A., Ashraf, S., Abbas, Q., Ahmed, A., and others,. Synthesis, X-ray crystal structure elucidation and Hirshfeld surface analysis of N-((4-(1 H-benzo [d] imidazole-2-yl) phenyl) carbamothioyl) benzamide: Investigations for elastase inhibition, antioxidant and DNA binding potentials for biological applicati. RSC. Adv. 2020;10(35):20837-20851.

45. Yan, Y., Lin, J., Xu, T., Liu, B., Huang, K., Qiao, L., Liu, S., Cao, J., Jun, S. C., Yamauchi, Y., and others,. Atomic-level platinum filling into Ni-vacancies of dual-deficient NiO for boosting electrocatalytic hydrogen evolution. Adv. Energy Mater. 2022;12(24):2200434.

46. Rahman H, Bintang MI, Asnawi A, Febrina E. Exploring the Molecular Interactions between Volatile Compounds in Coconut Shell Liquid Smoke and Human Bitter Taste TAS2R46 Based on the Molecular Docking and Molecular Dynamics. Trop. J. Nat. Prod. Res. 2023;7(12): 5587.

47. Karima R, Elya B, Sauriasari R. Mechanism of Action of Glucomannan as a Potential Therapeutic Agent for Type 2 Diabetes Mellitus Based on Network Pharmacology and Molecular Docking Simulation. Trop. J. Nat. Prod. Res. 2023;7(12): 5460.